TITLE: Airfoil and Wing Planform Optimization for
Micro Air Vehicles

TITLE: Aerodynamic Design and Optimisation of
Flight Vehicles in a Concurrent
Multi-Disciplinary Environment [la Conception et
l'optimisation aerodynamiques des vehicules
aeriens dans un environnement pluridisciplinaire
et simultane]

Airfoil and Wing Planform Optimization for Micro Air Vehicles

J. G. Sloan, W. Shyy* and R. T. Haftka

*University of Florida
Department of Aerospace Engineering, Mechanics & Engineering Science
P.O. Box 116250
Gainesville, Florida 32611-6250, U.S.A.

ABSTRACT

Low Reynolds number flight for micro air vehicles (μAVs) suffers from laminar separation resulting in reduced lift and increased drag. The objective of the present work is to use the response surface methodology (RSM) to identify correlations between the airfoil and the wing planform to facilitate a two-level optimization procedure in which an optimized airfoil and wing planform are reached simultaneously. Several approaches have been considered in this work. (1) A constant cross-section wing is modeled with maximum camber, y_c, maximum thickness, y_t, and aspect ratio, AR, as design variables at two different Reynolds numbers of 8.0×10^4 and 2.0×10^5. This is done to determine how the optimal airfoil may change for different aspect ratios and Reynolds numbers. (2) A variable cross-section wing defined by root camber and angle-of-attack and tip camber and angle-of-attack is modeled in order to determine how the optimal airfoil may change from the root to the tip of the wing. (3) Due to the size restrictions on μAVs, a fixed-span approach is used to model an aircraft subject to the constraints of steady flight with the aspect ratio and camber as design variables. This third approach balances trade-offs between wing area, aspect ratio, and Reynolds number in determining the overall flight efficiency. Optimal airfoils exhibit characteristics which change little with wing aspect ratio or location on the wing planform. There appears to be a trend of increasing optimal camber with decreasing Reynolds number. While the optimal design seems to favor airfoils with minimum thickness and relatively modest camber of about 4 to 5% of the chord, a higher camber may be a better choice if higher lift coefficient at minimum power is used as a design goal. Measurements of both the global and the local response surface prediction accuracy combined with design space refinement help to assess the reliability of the response surface approximations and optimal design predictions.

1. INTRODUCTION

The low-Reynolds number flight regime of micro air vehicles (μAVs) presents substantial aerodynamic design challenges. Micro air vehicles have length scales under 15 cm and flight speeds of approximately 15 m/s, resulting in Reynolds numbers between 10^4 and 10^5. Airfoil performance at these chord Reynolds numbers suffers from laminar separation and increased sensitivity to changing flow conditions. The increased sensitivity of the flow structure is important since fluctuations in wind velocity are comparable to the flight speed in this regime[1]. Furthermore, since airfoil performance decreases as Reynolds number decreases, attempts to shrink the overall aircraft size while trying to keep a 'workable' chord Reynolds number and sufficient lifting area result in low aspect ratio wing planforms[2]. As the aspect ratio decreases, the percentage of the wing area affected by wing-tip vortices increases, resulting in a largely three-dimensional flow field over most of the wing. An accurate analysis must consider the performance effects of both the airfoil geometry and the wing planform geometry.

The objective of the present study is to optimize airfoil and wing geometries for this flight regime using response surface methodology (RSM)[3]. RSM integrates statistical experimental design fundamentals, regression modeling techniques, and elementary optimization methods. Polynomial approximations are created relating aerodynamic performance measures to the variables which define the wing configuration. The number and the distribution of design points used for fitting response surfaces plays a large role in their predictive accuracy. The various design point selection techniques used in this study have been discussed and compared by Giunta et al.[4] and Unal et al.[5] for aerodynamic approximations in aerospace vehicle design. Design space refinement can improve the response surface prediction accuracy in the region of interest. Narducci et al.[6] and Sobieski et al.[7] used response surfaces fit to successively refined regions around the optimum. Other examples of RSM applied to fluid design problems are given in Madsen et al.[8], Knill et al.[9], and Baker et al.[10].

Since a common obstacle encountered during μAV design is the weight of the onboard energy supply, minimizing the flight power consumption is an appropriate design objective. Attempts are made to identify correlations between the airfoil and the wing planform to facilitate a two-level optimization procedure in which an optimized airfoil is found for an optimized wing planform. Design variables are chosen based on their ability to modify the flow fields under consideration. Governing flow quantities such as mass and momentum fluxes are strongly influenced by wing camber, thickness, aspect ratio, and angle-of-attack. Additionally, flow fields in the Reynolds number range of currently envisioned μAVs are largely dependent on the Reynolds number and freestream disturbance level[11].

Several approaches have been considered in this work. (1) A constant cross-section wing is modeled with maximum camber, y_c, maximum thickness, y_t, and aspect ratio, AR, as design variables at two different Reynolds numbers of 8.0×10^4 and 2.0×10^5. This is done to determine how the optimal airfoil may change for different aspect ratio wings and different Reynolds numbers. Investigations of the sensitivity of optimal camber with changes in the flight Reynolds number may warrant and facilitate the use of a variable camber airfoil. (2) A variable cross-section wing defined by root camber and angle-of-attack and tip camber and angle-of-attack is modeled in order to determine how the optimal airfoil may change from the root to the tip of the wing. (3) Due to the size restrictions on μAVs, a fixed-span approach is

Paper presented at the RTO AVT Symposium on "Aerodynamic Design and Optimisation of Flight Vehicles in a Concurrent Multi-Disciplinary Environment", held in Ottawa, Canada, 18-21 October 1999, and published in RTO MP-35.

used to model an aircraft subject to the constraints of steady flight with the aspect ratio and camber as design variables. This third approach balances trade-offs between wing area, aspect ratio, and Reynolds number in determining the overall flight efficiency.

Accurate evaluations of low Reynolds number airfoils require aerodynamic models which take into account the performance effects of separation and laminar-turbulent transition. Although precise modeling of the flow structure associated with separation requires a solution of the full Navier-Stokes equations, the effects of thinly separated regions on pressure and viscous shear forces can usually be substantially captured by reduced-equation boundary layer models[12,13]. Such a reduced two-dimensional model combined with a three-dimensional potential flow solver is incorporated in the present study to make an incremental design/optimization procedure feasible.

2. PERFORMANCE CRITERIA

The performance analysis is based on both a three-dimensional potential flow solution provided by *PMARC*[14] and a two-dimensional inviscid/boundary-layer solution (also referred to as viscous/inviscid solution) for the airfoil provided by *XFOIL*[15,12]. Performance is measured by the power index, $C_L^{3/2}/C_D$, which appears explicitly in the equation for the steady flight power requirement, P_r, given by[16,17,18]

$$P_r = \frac{C_D}{C_L^{3/2}} \sqrt{\frac{2W^3}{\rho S}} \tag{1}$$

The lift coefficient, C_L, is the non-dimensional force component perpendicular to the freestream velocity vector. The drag coefficient, C_D, is the non-dimensional force component parallel to the freestream velocity vector. In Eq. (1), W, ρ, and S are, respectively, aircraft weight, air density, and wing reference area.

The drag coefficient, C_D, will be discussed in terms of three drag component coefficients such that

$$C_D = C_{d_f} + C_{d_p} + C_{d_i} \tag{2}$$

where

1) C_{d_f} is known as the frictional drag coefficient, and it results from fluid forces which act tangentially to the airfoil surface due to viscosity and velocity gradients at the solid surface,

2) C_{d_p} is known as the pressure drag coefficient (or alternatively as form drag or afterbody drag), and it results from fluid forces which act normal to the airfoil surface, and

3) C_{d_i} is known as the induced drag coefficient, and it results from a change in the relative wind over the wing from lift-induced wing-tip vortices.

The sum of the friction drag and the pressure drag is commonly known as the 'profile drag'. Since C_{d_f} is a result of viscous shear forces, and the inviscid solution around an arbitrary, 2-D configuration gives a resultant force perpendicular to the freestream, leaving $C_{d_p} = 0$, the profile drag can be termed the viscous drag. The C_{d_p} component of the viscous drag results from modification to the effective airfoil shape caused by boundary layer thickness, separation and the trailing wake.

In the following analyses, the lift coefficient is determined from *PMARC*, and the drag coefficient is determined by adding the profile drag coefficient given by *XFOIL* and the induced drag coefficient given by *PMARC*. The average profile drag is used for wings with varying cross-section, which offers an approximate estimate with much reduced computing needs.

XFOIL simulates inviscid or coupled inviscid/boundary-layer flow around 2-D airfoils. *XFOIL*'s predictive accuracy was assessed in Shyy et al.[13]. *XFOIL* uses a two-equation boundary layer integral formulation based on dissipation closure for both laminar and turbulent flows[12]. A two-equation model is necessary in order to uniquely determine the shape parameter in separated flow regions. *XFOIL* also employs the e^n laminar-turbulent transition prediction model[19,20,21]. The e^n method is based on linear stability analysis using the Orr-Sommerfeld equation to determine the growth of spatially developing waves.

XFOIL determines the lift coefficient from integration of surface pressures, where the surface pressures are obtained from the potential flow solution. The drag coefficient is calculated from the Squire-Young formula[22,23],

$$C_d = \frac{2\theta_\infty}{c}, \tag{3}$$

where θ_∞ is the wake momentum thickness at downstream infinity and c is the airfoil chord. The Squire-Young formula is obtained by applying the momentum theorem to a control volume surrounding the airfoil, and it measures the fluid momentum losses downstream of the airfoil. This measurement provides the 2-d profile drag of the airfoil, namely, $C_d = C_{d_f} + C_{d_p}$.

PMARC is a low-order potential flow panel code for three-dimensional geometries in unsteady flow fields. Laplace's equation for the velocity potentials is resolved by superposition of source and doublet solutions throughout the wing surface and trailing wake. The lift coefficient is determined from integration of surface pressures, and the induced drag coefficient is determined by Trefftz plane analysis[24].

PMARC's accuracy was tested against *XFOIL* for three different airfoils: the two well-known airfoils, NACA 0012 and CLARK-Y, and a recently proposed low Reynolds number airfoil, S1223[25]. The three airfoils and the results of the assessment are presented by Sloan[26].

3. THE RESPONSE SURFACE METHOD

The approach of RSM is to perform a series of experiments, or numerical analyses, for a prescribed set of design points, and to construct a global approximation (response surface) of the measured quantity (the response) over the design space. In the present context, the response is a measure of wing performance such as $C_L^{3/2}/C_D$, and the design space consists of a set of relevant design variables such as camber, thickness, angle-of-attack, and so on. Quadratic polynomials are used for the response surface approximations for which extremal points are easily found by standard constrained optimization algorithms. The main advantages of RSM over other optimization tools such as gradient-based search algorithms are that it requires minimal interfacing with the analysis tools and avoids the need for expensive derivative calculations. However, RSM is practically limited by the number of design variables which can be considered. A response surface represented by a quadratic polynomial has $(k+1)(k+2)/2$ coefficients, where k is the number

of design variables. So, for example, a quadratic polynomial in 10 variables has 66 coefficients which requires an even higher number of analyses to obtain a reliable fit.

The response surface is fit by standard least squares regression using *JMP*[27] statistical analysis software. *JMP* is an interactive, spreadsheet-based program which provides a variety of statistical analysis functions. A *backward elimination* procedure based on t-statistics is used to discard terms and improve the prediction accuracy[3]. The t-statistic, or t-ratio, is given by

$$t_o = \frac{b_j}{se(b_j)}, \tag{4}$$

where b_j is the regression coefficient and $se(b_j)$ is the standard error of the regression coefficient. The standard error of the regression coefficient is given by

$$se(b_j) = \hat{s}\sqrt{C_{jj}} \tag{5}$$

where $\hat{s}$ is an unbiased estimator of the standard deviation of the observations (also an unbiased estimator of the rms error in prediction based on the response surface) and C_{jj} is the diagonal element of $(\boldsymbol{X}'\boldsymbol{X})^{-1}$ corresponding to b_j. The standard deviation, $\hat{s}$, is given by

$$\hat{s} = \sqrt{\frac{\sum e_i^2}{n-p}} \tag{6}$$

where the residual, e_i, is the difference between the observation, y_i, and the fitted value, $\hat{y}_i$. $\boldsymbol{X}$ is an $n \times p$ matrix of the levels of the independent variables where n is the number of observations and p is the number of terms in the model. In the present case, $\boldsymbol{X}$ is a 27×10 matrix representing 27 levels of the 10-term model resulting from 27 combinations of the 3 design variables. Looking for a t-statistic > 2 in absolute value is a common rule of thumb since this value corresponds to an approximately 5 percent probability of mistakenly rejecting the null hypothesis that the coefficient is zero. In the backward elimination procedure, the acceptable probability for leaving a term in the model is usually changed until the most accurate reduced model is found. Additionally, it is common to retain linear terms with unacceptable t-statistics if they are included in significant higher-order terms. The global fit and prediction accuracies of the full and reduced response surfaces are assessed through statistical measures such as R^2, R_a^2, and $\hat{s}$.

The R^2 value is determined by

$$R^2 = \frac{SS_R}{SS_{yy}} = 1 - \frac{SS_E}{SS_{yy}} \tag{7}$$

where SS_E is the sum of squares of the residuals ($\sum e_i^2$) or errors, SS_R is the sum of squares due to regression, and SS_{yy} is the total sum of squares about the mean, where

$$SS_{yy} = SS_R + SS_E \tag{8}$$

R^2 measures the proportion of the variation in the response around the mean that can be attributed to terms in the model rather than to random error. R_a^2 is an R^2 value adjusted to account for the degrees of freedom in the model and is given by

$$R_a^2 = 1 - \frac{SS_E/(n-p)}{SS_{yy}/(n-1)} = 1 - \left(\frac{n-1}{n-p}\right)(1-R^2). \tag{9}$$

Since R^2 will always increase as terms are added to the model, the overall assessment of the model may be better judged from R_a^2, since it will often decrease if unnecessary terms are added.

Similar to R_a^2, $\hat{s}$ is corrected for the degrees of freedom in the model. Even though a full response surface with a higher value of R^2 fits the variability in the data better, one or more reduced response surfaces may have higher values of R_a^2 and lower values of $\hat{s}$ making them better predictors. Support for this measure is based on the idea that there is a danger in retaining terms with low t-statistics since the extra degrees of freedom may be fitting noise.

4. OPTIMIZATION OF AIRFOIL SHAPE AND ASPECT RATIO: y_c, y_t, and AR

Shyy et al.[13] have conducted computer analysis which suggests that increased camber and reduced thickness are beneficial to low Reynolds number ($Re = 7.5 \times 10^4$ to 3.0×10^5) airfoil flows. Similar results were obtained experimentally by Jenkins et al.[28] at $Re = 2.0 \times 10^4$ to 1.0×10^5. Experiments conducted by Sunada et al.[29] at a much lower Reynolds number of $Re = 4.0 \times 10^3$ also indicate that airfoils at this Reynolds number should be relatively thin and well-cambered. Their best airfoil as measured by C_L/C_D had 5% camber, whereas their best airfoil as measured by $C_L^{3/2}/C_D$ had 10% camber. However, in these studies, no attempt has been made to optimize the wing and airfoil shapes based on a systematic approach. In this regard, the response surface method (RSM)[3] is used here to determine optimal values of camber and thickness for different aspect ratio wings.

The three design variables initially considered for optimization are the maximum camber, y_c, maximum thickness, y_t, and the wing aspect ratio, AR. The NACA surface distribution is used to create the airfoils based on maximum camber and maximum thickness, where the position of the maximum camber was chosen to be at 40% of the chord. The three design variables are constrained to the following ranges:

$$0.0 \le y_c \le 0.10c$$
$$0.05c \le y_t \le 0.15c$$
$$1 \le AR \le 5$$

The reason for the lower bound on y_t is that convergent *XFOIL* solutions are not obtainable for many airfoils with thicknesses less than 5%, due to numerical ill-conditioning in the potential flow calculation. The analyses are done for both $Re = 2.0 \times 10^5$ and $Re = 8.0 \times 10^4$. A full-quadratic response surface representing this design space consists of 10 terms and is evaluated by analyses of the 27 points of the full three-level factorial design. The response is chosen to be the maximum power index, $C_L^{3/2}/C_D$. The maximum power index for each of the 27 design points is determined by calculating the power index at successively narrower ranges and finer resolutions of angle-of-attack in the vicinity of the maximum. The design

variables are scaled to lie in the range -1 to 1 which improves the numerical conditioning of the problem. Tables 1 and 2 list the coefficients and their associated t-statistics along with values of R^2, R_a^2, and $\hat{S}$ for both the full and reduced response surfaces for Re=2.0 × 10^5 and Re=8.0 × 10^4 respectively. Both reduced models in Tables 1 and 2 provide improved values of R_a^2 and $\hat{s}$ over the full models and are chosen for optimization.

The equation describing the response as given by *JMP* is input to *Solver*[30]. *Solver* is an optimization toolbox included with Microsoft Excel which uses the Generalized Reduced Gradient method to find the maximum or minimum of a function with given constraints. Tables 3 and 4 list the maximum $C_L^{3/2}/C_D$ and the corresponding camber for aspect ratios of AR = 1,3, and 5. All optimal airfoils had a thickness of 5%, the lowest allowable value set by the constraints. The predicted response value in Tables 3 and 4 is the response value given from the response surface approximation. The actual response value is the response value obtained by reanalyzing the optimal point given by the response surface approximation. The angle-of-attack listed in Tables 3 and 4 is the angle-of-attack at which the actual response value occurs. The best maximum $C_L^{3/2}/C_D$ values for each aspect ratio from the original data used to construct the response surfaces are also listed. The original data for all of the response surfaces in this paper can be found in Ref. [26].

From the original 27 data points used to fit the response surface at Re = 2.0 × 10^5 the airfoil corresponding to y_c = 0.05 and y_t = 0.05 gives superior performance over the predicted optima for AR = 1, 3, and 5 in Table 3. The same airfoil also gives superior performance over the optima in Table 4 at Re = 8.0 × 10^4. The fact that the response surfaces could not predict an optimal point at least as good as one of the original data reveals their poor prediction accuracy. Figures 1 and 2 show the response surface approximations plotted against actual values taken from Tables 3 and 4 and from the nine original design points in the plane at y_t = 0.05 of the full three-level factorial design used to construct the response surfaces. These figures show that the response surfaces are not capturing the actual peak in the data.

The actual errors for the optimal points listed in Table 3 for Re = 2.0 × 10^5 are all smaller than the predicted rms error of 0.619 for that response surface, showing that the prediction accuracy of the response surface at these points is at least as good as expected. However, two of the optimal points listed in Table 4 (the points at AR = 1 and AR = 5) for Re = 8.0 × 10^4 have actual errors larger than the predicted rms error of 0.655 for that response surface.

The estimated standard error of a predicted response at some location $\boldsymbol{x}$ is given by

$$s_{\hat{y}(\boldsymbol{x})} = \hat{s}\sqrt{\boldsymbol{x}^{(m)'}(\boldsymbol{X}'\boldsymbol{X})^{-1}\boldsymbol{x}^{(m)}} \qquad (10)$$

where $\hat{s}$ is the rms error, $\boldsymbol{x}^{(m)}$ is a vector which is a function of the location where the *(m)* notation indicates that $\boldsymbol{x}^{(m)}$ has been expanded to "model space" to reflect the form of the model as $\boldsymbol{X}$ does. For example, in the present case $\boldsymbol{x}^{(m)}$ for the full model is given by

$$\boldsymbol{x}^{(m)'} = [1, y_c, y_t, AR, y_c^2, y_t y_c, y_t^2, ARy_c, ARy_t, AR^2]. \qquad (11)$$

The estimated standard errors for the two overly inaccurate points in Table 4 are both 0.327. The actual error is larger than both the predicted rms error and the local estimated standard error at these optimum. It follows that the actual error at these two disappointing optimal points could not have been anticipated based on rms error or local estimated standard error. It appears that the variation in the response over the chosen design space cannot be sufficiently modeled with a quadratic polynomial.

In order to obtain more reliable fits, the design space is reduced by first setting the thickness, y_t, equal to 5% and fitting six separate response surfaces in the single variable camber, y_c, for aspect ratios of AR = 1, 3, and 5 for each Reynolds number. The five design points of y_c = 0.02, 0.03, 0.04, 0.05, and 0.06 are chosen to fit each response surface. The six response surfaces along with their values of R^2, R_a^2, and $\hat{s}$ are shown in Table 5. In all cases, reduced models did not improve the prediction accuracy. The optimal points predicted by the six response surfaces are listed in Table 6.

The six response surfaces presented in Table 5 all have excellent values of R^2, R_a^2, and $\hat{s}$. All predicted optima in Table 6 are very accurate and all happen to be very close in response value to a design point in the original data. The results show that the optimal camber changes very little with changes in wing aspect ratio over this range. The predicted optimal camber appears to increase by about 0.5% of the chord when the Reynolds number decreases from Re = 2.0 × 10^5 to Re = 8.0 × 10^4. The best maximum $C_L^{3/2}/C_D$ from the raw data also occur at a higher camber on average at Re = 8.0 × 10^4. Overall, it appears from the results in Table 6 that an airfoil with 4% camber and 5% thickness would provide superior performance over this range of flight conditions.

The modest optimal cambers obtained in Table 6 seem to contradict the conclusions of Ref. [13] which suggest that low Reynolds number airfoils should have relatively high camber. In order to determine why modest cambers are favored by the 3-D model, curves of $C_L^{3/2}/C_D$ as a function of angle-of-attack for four different wings at different aspect ratios and different cambers are shown in Figure 3. As can be seen at aspect ratios of both AR = 1 and AR = 5 the wings with 5% camber exhibit a higher maximum $C_L^{3/2}/C_D$ than the 8% camber wings even though both wings have comparable overall performance. The peaks in the $C_L^{3/2}/C_D$ vs. α curves are due to a sudden drop in the profile drag coefficient, C_d, at the corresponding angle-of-attack as can be seen in Figure 4. The sudden change in C_d looks suspicious and may be largely noise. At AR = 5, both the 5% and 8% camber airfoils provide nearly the same overall performance. At AR = 1, the $C_L^{3/2}/C_D$ vs. α curves are very flat and the difference in performance between the two airfoils is practically negligible. With such similar performance between the two airfoils, the data of Figure 3 is fit with quadratic polynomials to see if the smoothing effect of the least-squares fit changes the curves enough to result in a different optimum airfoil. The polynomials are plotted in Figure 5 and show that the 5% camber airfoil remains superior after filtering the noise, while the 8% camber airfoil exhibits more steady performance with regard to the change in the angle-of-attack.

Figure 6 shows plots of the lift coefficient, C_L, vs. α for the four wings. The 8% camber airfoil provides superior lift at both aspect ratios. With both the 5% and 8% camber airfoils providing similar power requirements, the 8% camber airfoil may be the better choice if the lift coefficient at minimum power is taken into consideration.

Figure 7 shows pressure distributions at 3 different spanwise locations for wings of $AR = 1$ and $AR = 5$ with a NACA 5405 airfoil and $\alpha = 5°$. The root section and mid-span section pressure distributions for each aspect ratio are nearly the same, showing that the flow is two-dimensional in that region. However, the magnitude of the section lift coefficients along the span as represented by the area between the upper and lower pressure curves is significantly reduced as the aspect ratio decreases. Thus, the spill-over effects at the wing-tips are felt along the entire span at low aspect ratios. Therefore, it can be expected that the 3-D optimal airfoil is different from the 2-D one.

5. SPANWISE DESIGN VARIATION: y_{cr}, y_{ct}, α_r, and α_t

In order to test how the optimal airfoil should vary with spanwise location, a procedure is developed which includes four design variables. The design variables are chosen to be the root camber and root angle-of-attack designated by y_{cr} and α_r, and the tip camber and tip angle-of-attack designated by y_{ct} and α_t. The wing thickness is set at 5%. The response is the power index, $C_L^{3/2}/C_D$, and the analyses are done at $Re = 8.0 \times 10^4$ and $AR = 1$. The ranges of the design variables are chosen to encompass the predicted optimal point for $AR = 1$ in Table 4. Such ranges are as follows:

$0.05c \le y_{cr} \le 0.10c$ $\quad$ $0.05c \le y_{ct} \le 0.10c$

$2.5° \le \alpha_r \le 7.5°$ $\quad$ $2.5° \le \alpha_t \le 7.5°$

This range was selected before the design space refinement resulting in the optimal points of Table 6. However, this range includes the best point from the raw data at $Re = 8.0 \times 10^4$ and $AR = 1$. The points selected to fit the response surface are the 25 points of a 4-dimensional central-composite design. The equation of the best reduced response surface along with its values of R^2, R_a^2, and $\hat{s}$ and its predicted optimum are shown in Table 7.

The predicted optimal camber and angle-of-attack values decreased from root to tip. However, the actual optimal $C_L^{3/2}/C_D$ is lower than six of the response values used in the response surface construction. The actual error at the optimal point listed in Table 7 could not have been anticipated since it is substantially larger than both the predicted rms error of 0.127 and the local standard error at the optimum of 0.083. Again it appears that a quadratic polynomial cannot sufficiently model the variation in the response for the range of design variables considered.

After reviewing the data used to fit the response surface and identifying design points with relatively high values of the response, the design space is reduced considerably by narrowing the ranges of the design variables to the following:

$0.05c \le y_{cr} \le 0.10c$ $\quad$ $0.05c \le y_{ct} \le 0.075c$

$5° \le \alpha_r \le 7.5°$ $\quad$ $2.5° \le \alpha_t \le 5°$

Additionally, the number of design points used to construct the response surface is increased to 30. The 30 points are chosen by first generating the 81 points of the full three-level factorial design and using the D-optimality criterion[3] for selecting 30 of these 81 points. The best reduced response surface and its predicted optimum are shown in Table 8.

The optimal point selected in Table 8 corresponds to the best design point from the 30 design points used to fit the response surface. Reducing the design space resulted in improved prediction accuracy. The rms-error of the response surface in Table 8 is relatively low showing that the quadratic form fits the data rather well over this reduced size design space. In an attempt to further improve the optimal design, the next step retains the size of the design space but shifts it so that the best point in Table 8 is now the center of the design space, resulting in the following ranges for the design variables:

$0.025c \le y_{cr} \le 0.075c$ $\quad$ $0.0375c \le y_{ct} \le 0.0625c$

$3.75° \le \alpha_r \le 6.25°$ $\quad$ $3.75° \le \alpha_t \le 6.25°$

Five of the design points used to fit the response surface in Table 8 lie in the full three-level factorial design of the current design space and are used in the fit. An additional 25 points are selected from the remaining points in the full three-level factorial design based on the D-optimality criterion. The best reduced response surface and its predicted optimum are shown in Table 9.

The optimal point obtained in Table 9 has a lower actual response value than the best point in the raw data which was selected as the optimum in Table 8. Centering the design space about the optimal point did not improve the prediction accuracy around that point sufficiently enough to identify a better optimum. Adding the flexibility of a variable cross section has not resulted in an improved optimal design for reasons that are unclear. The results identify an optimal wing geometry as having a constant cross section of 5% camber which corresponds to the results in Table 6 for $AR = 1$ and $Re = 8 \times 10^4$.

6. OPTIMIZATION OF FIXED-SPAN WING IN STEADY FLIGHT: y_c and AR

It is apparent that maximum performance will always occur at the highest aspect ratio, which for a given chord Reynolds number means maximizing the span. However, in practice, size restrictions place limits on the span. In this section, the aspect ratio remains a variable, but the span is fixed at 10 inches (25.4 cm). This procedure makes the chord, and therefore the chord Reynolds number, an implicit design variable.

The optimization problem is formulated in the two design variables camber and aspect ratio with the thickness set at 5%. The initial ranges of the design variables are the following:

$0.0 \le y_c \le 0.10c$

$0.5 \le AR \le 1.5$

Since the wing area, S, varies with aspect ratio, an appropriate response for minimizing the power requirement is the maximum $C_L^{3/2} \cdot S^{1/2}/C_D$ from Eqn. (1). The aircraft weight, W, is set at 16 oz, and the available thrust power, P_a, is set at 28 watts. The aircraft is modeled in steady flight flying at the minimum power velocity, V_{min}. Steady flight is defined by the following relations:

$$L = W \tag{12}$$

$$T = D \tag{13}$$

Equation (12) can be rearranged to obtain the required flight velocity as,

$$V_{\min} = \sqrt{\frac{2W}{\rho S C_L}} \tag{14}$$

For each design point, values for ρ, W, and S are given and C_L (from *PMARC*) is determined independently of the Reynolds number and is therefore only a function of the geometry and the angle-of-attack. Substituting the lift coefficient at minimum power, $C_{L_{minp}}$, into Eqn. (14) gives the minimum power velocity, V_{minp}.

Equation (13) can be rearranged to obtain an expression for the maximum sustainable velocity as,

$$V_{\max} = \sqrt[3]{\frac{2P_a}{\rho S C_{D_{minp}}}} \qquad (15)$$

Since the velocity from Equation (14) now determines the Reynolds number, an *XFOIL* solution for the given airfoil at this Reynolds number will complete the calculation for the flight C_D (C_{d_i} is already given from the *PMARC* solution). The design is feasible as long as the minimum power velocity is less than or equal to the maximum sustainable velocity.

In order to determine the maximum $C_L^{3/2} \cdot S^{1/2}/C_D$ for a given wing subject to the constraints of steady flight, an iteration procedure is set up by first guessing a Reynolds number and calculating an initial maximum $C_L^{3/2}/C_D$. The lift coefficient at the initial maximum $C_L^{3/2}/C_D$ will determine the initial V_{minp}. With an initial V_{minp} in hand, a new Reynolds number and a new maximum $C_L^{3/2}/C_D$ can be determined. This procedure converges when the current maximum $C_L^{3/2}/C_D$ occurs at a $C_{L_{minp}}$ and V_{minp} creating the same Reynolds number at which the maximum $C_L^{3/2}/C_D$ is being determined. Typically, the procedure requires between 3 and 7 iterations.

The first response surface is fit using the 9 points of a two-dimensional central composite design shown as Set A design points in Figure 8. According to the flow model calculations, all aircraft in the range of design variables considered are able to fly in steady flight. The full response surface fit to Set A design points is presented as the Set A response surface in Table 10. Reduced models did not improve the prediction accuracy.

Evaluation of the Set A response surface gives an optimal response value of 1.257 m at $y_c = 0.0639$ and $AR = 1.5$. The actual response value for this design is 1.213 m. The discrepancy between the predicted an actual response value along with the observation that aspect ratio was maximized suggests that refinement of the design space may improve the prediction accuracy and the final design. Five successively refined sets of response surface design points are shown in Figure 8. The design points are marked with filled circles and the optimal points predicted by the response surfaces fit to each set of design points are marked with an X. Response surface data for Sets B through E are shown in Table 10. In all cases, reduced response surfaces do not improve the prediction accuracy and are not shown. However, Sets D and E which include only the design variable y_c, found a much better fit with a cubic polynomial rather than a quadratic polynomial. Predicted and actual optimal response values for Sets A through E are shown in Table 11.

Each step of the design space refinement consistently improved the actual optimal design performance. The final optimal design of $AR = 1.5$ and $y_c = 0.0295$ has a chord Reynolds number of $Re = 3.09 \times 10^5$ when flying at its minimum power velocity of $V_{minp} = 27.2$ m/s. The improvements in $C_L^{3/2}/C_D$ for the higher aspect ratio wings outweighed the negative effects from their smaller area, S. The smaller area wings compensate to meet the steady flight constraints by flying at a slightly higher velocity.

Table 12 shows the rms error and local standard error along with the actual error for the optimal designs for each design point set. It again appears that neither the rms error nor the estimated local standard error provide a reliable way to predict the actual error at the optimum. Also, after reviewing the data used to fit the response surface, it is apparent that the two steps in the design space refinement represented by Sets B and C would not have been necessary if the raw data had been considered when choosing a refined region. The predicted optimum from the Set A response surface is lower than the actual response value in Set A corresponding to $y_c = 0.05$ and $AR = 1.5$. This design point was not predicted as an optimum from a response surface approximation until Set C. A refinement procedure which only follows the predicted optimum, instead of also considering the original data, can result in additional refinement steps.

A single response surface was fit to all of the design points contained in Sets A-E and the best reduced model and its predicted optimum is presented in Table 13. The single response surface fit to all of the design points in Sets A-E had lower values of R^2 and R_a^2 and a higher rms error than any of the response surfaces presented in Table 10. The single response surface fit to all of the design points in Sets A-E spanning the entire initial design space does not provide sufficient predictive accuracy.

7. CONCLUSION

The response surface method has been used to investigate and identify optimal wing geometries providing minimum power consumption for low Reynolds number flight vehicles. In all cases, optimization provided only a modest improvement in the flight power requirement. However, some insight was gained into particular trends concerning low-Reynolds-number, low-aspect-ratio wing design. As anticipated, the wing thickness should be minimized. The results of Table 6 suggest that optimal airfoils change very little with changes in wing aspect ratio. Investigations into how the optimal airfoil changes with spanwise location revealed that the best wing had a constant cross-section with 5% camber oriented at 5° angle-of-attack. The optimal airfoil is not strongly coupled to the wing planform since it does not change much with changes in aspect ratio or with location on the wing. The analyses of Sections 3 and 4 suggest that optimal cambers lie at about 4% or 5%. The fixed-span, steady flight calculations in Section 5 resulted in optimal cambers being significantly lower at about 3%, albeit at a higher Reynolds number. There appears to be a trend of increasing optimal camber with decreasing Reynolds number. Furthermore, a higher camber may be a better choice if higher lift coefficient at minimum power is used as a design goal, instead of simply minimizing the overall power index.

Obtaining accurate response surface approximations requires using an appropriate number of design points for the model being fitted. For some of the response surface approximations created in this work, such as in the first spanwise cross-section variation problem, using too few points may have contributed to the poor prediction accuracy. Also, the original

data as well as the predicted optimum should be considered when conducting a zooming procedure for design space refinement.

8. REFERENCES

1) Liu, H.-T. (1992). Unsteady aerodynamics of a Wortmann wing at low Reynolds numbers. *Journal of Aircraft, 29*, 532-539.

2) Handley, C. (1998, July-August). Tiny planes, big tasks. *Compressed Air*, pp. 14-20.

3) Myers, R. H., & Montgomery, D. C. (1995). *Response surface methodology - process and product optimization using designed experiments.* New York: John Wiley & Sons, Inc.

4) Giunta, A. A., Dudley, J. M., Narducci, R., Grossman, B., Haftka, R. T., Mason, W. H., & Watson, L. T. (1994). Noisy aerodynamic response and smooth approximations in HSCT design. AIAA Paper No. 94-4376.

5) Unal, R., Lepsch, R. A., & McMillin, M. L. (1998). Response surface model building and multidisciplinary optimization using D-optimal designs. AIAA Paper No. 98-4759.

6) Narducci, R., Valorani, M., Dadone, A., Grossman, B., & Haftka, R. T. (1995). Optimization methods for non-smooth or noisy objective functions in fluid design problems. AIAA Paper No. 95-1648.

7) Sobieski, I. P., Manning, V. M., & Kroo, I. M. (1998). Response surface estimation and refinement in collaborative optimization. AIAA Paper No. 98-4753.

8) Madsen, J. I., Shyy, W., Haftka, R. T., & Liu, J. (1997). Response surface techniques for diffuser shape optimization. AIAA Paper No. 97-1801.

9) Knill, D. L., Giunta, A. A., Baker, C. A., Grossman, B., Mason, W. H., Haftka, R. T., & Watson, L. T. (1998). HSCT configuration design using response surface approximations of supersonic euler aerodynamics. AIAA Paper No. 98-0905.

10) Baker, C. A., Grossman, B., Haftka, R. T., Mason, W. H., & Watson, L. T. (1998). HSCT configuration design space exploration using aerodynamic response surface approximations. AIAA Paper No. 98-4803.

11) Mueller, T. J. (Ed.) (1989). *Low Reynolds number aerodynamics.* New York: Springer-Verlag.

12) Drela, M., & Giles, M. B. (1987). Viscous-inviscid analysis of transonic and low Reynolds number airfoils. *AIAA Journal, 25*(10), 1347-1355.

13) Shyy, W., Klevebring, F., Nilsson, M., Sloan, J., Carroll, B., & Fuentes, C. (1999). A Study of Rigid and Flexible Low Reynolds Number Airfoils. *Journal of Aircraft*, 36(3), 523-529.

14) Ashby, D. L., Dudley, M. R., Iguchi, S. K., Browne, L., & Katz, J. (1992). *Potential flow theory and operation guide for the panel code PMARC_12.* Computer Software Management and Information Center (COSMIC), University of Georgia.

15) Drela, M. (1989). XFOIL: An analysis and design system for low Reynolds number airfoils. In T. J. Mueller (1989) *Low Reynolds number aerodynamics.* New York: Springer-Verlag, pp. 1-12.

16) Anderson, J. D., Jr. (1989). *Introduction to flight.* (3rd ed.). New York: McGraw-Hill.

17) Donovan, J. F., & Selig, M. S. (1989). Low Reynolds number airfoil design and wind tunnel testing at Princeton University. In T. J. Mueller (1989) *Low Reynolds number aerodynamics.* New York: Springer-Verlag, pp. 39-57.

18) Foch, R. J., & Ailinger, K. G. (1992). Low Reynolds number, long endurance aircraft design. AIAA Paper No. 92-1263.

19) Smith, A. M. O., & Gamberoni, N. (1956). Transition, pressure gradient, and stability theory. Douglas Aircraft Co., Rept. ES 26388.

20) Ingen, J. L. van (1956). A suggested semi-empirical method for the calculation of the boundary layer transition region. Delft University of Technology, Dept. of Aerospace Engineering, Rept. VTH-74.

21) Cebeci, T., & Bradshaw, P. (1977). *Momentum transfer in boundary layers.* Washington: Hemisphere Publishing Corporation.

22) Squire, H. B., & Young, A. D. (1937). The calculation of the profile drag of aerofoils. *Reports and Memoranda Aeronautical Research Council, London*, No. 1838 (1938 Vol.).

23) Rosenhead, L. (Ed.) (1963). *Laminar boundary layers.* New York: Dover Publications, Inc.

24) Katz, J., & Plotkin, A. (1991). *Low-speed aerodynamics: from wing theory to panel methods.* New York: McGraw-Hill, Inc.

25) Selig, M. S., & Guglielmo, J. J. (1997). High-lift low Reynolds number airfoil design. *Journal of Aircraft, 34*(1), 72-78.

26) Sloan, J. G. (1998). Airfoil and Wing Planform Optimization for Low Reynolds Number Flight Vehicles. Master Thesis, Department of Aerospace Engineering, Mechanics & Engineering Science, University of Florida.

27) SAS Institute Inc. (1995). JMP version 3. Cary, N.C.

28) Jenkins, D. A., Shyy, W., Sloan, J., Klevebring, F., & Nilsson, M. (1998). Airfoil performance at low Reynolds numbers for micro air vehicle applications. RPVs Thirteenth International Conference, Bristol, United Kingdom.

29) Sunada, S., Sakaguchi, A., & Kawachi, K. (1997). Airfoil section characteristics at a low Reynolds number. *Journal of Fluids Engineering, 119*(1), 129-135.

30) Microsoft Corporation. (1985-1996). Microsoft Excel 97.

Table 1. Coefficients and corresponding t-statistics along with overall fit information for both the full and reduced response surfaces for maximum $C_L^{3/2}/C_D$ as a function of y_c, y_t, and AR at Re = 2.0 ×10^5.

term	coefficient (full)	t-stat (full)	coefficient (red.)	t-stat (red.)
intercept	9.332	28.45	9.211	34.59
y_c	0.8296	5.46	0.8296	5.69
y_t	0.1011	0.67	0.1011	0.69
AR	4.256	28.02	4.256	29.17
y_c*y_c	-1.578	-6.00	-1.578	-6.24
y_t*y_c	-0.6998	-3.76	-0.6998	-3.92
y_t*y_t	-0.1812	-0.69	-	-
*AR**y_c	0.3905	2.10	0.3905	2.19
*AR**y_t	0.0433	0.23	-	-
*AR***AR*	-0.5390	-2.05	-0.5390	-2.13
R^2	0.981		0.980	
R_a^2	0.971		0.973	
$\hat{s}$	0.644 (8.25% of mean)		0.619 (7.94% of mean)	

Table 2. Coefficients and corresponding t-statistics along with overall fit information for both the full and reduced response surfaces for maximum $C_L^{3/2}/C_D$ as a function of y_c, y_t, and AR at Re = 8.0 ×10^4.

term	coefficient (full)	t-stat (full)	coefficient (red.)	t-stat (red.)
intercept	7.778	23.00	7.778	23.33
y_c	0.3733	2.38	0.3733	2.42
y_t	-0.3678	-2.35	-0.3678	-2.38
AR	3.372	21.54	3.372	21.85
y_c*y_c	-1.600	-5.90	-1.600	-5.99
y_t*y_c	-0.9553	-4.98	-0.9553	-5.05
y_t*y_t	-0.3389	-1.25	-0.3389	-1.27
*AR**y_c	0.1314	0.69	-	-
*AR**y_t	-0.1916	-1.00	-	-
*AR***AR*	-0.4880	-1.80	-0.4880	-1.83
R^2	0.970		0.967	
R_a^2	0.953		0.955	
$\hat{s}$	0.664 (10.78% of mean)		0.655 (10.63% of mean)	

Table 3. Predicted and actual maximum $C_L^{3/2}/C_D$ with corresponding y_c for a given AR at Re = 2.0 ×10^5.

AR	y_c	$C_L^{3/2}/C_D$ predicted	$C_L^{3/2}/C_D$ actual	α (deg.)	Best $C_L^{3/2}/C_D$ from raw data
1.0	0.0680	4.52	4.04	1.7	4.12
3.0	0.0742	9.48	9.40	1.3	9.69
5.0	0.0804	13.41	13.63	1.3	14.09

Table 4. Predicted and actual maximum $C_L^{3/2}/C_D$ with corresponding y_c for a given AR at Re = 8.0 ×10⁴.

AR	y_c	$C_L^{3/2}/C_D$ predicted	$C_L^{3/2}/C_D$ actual	α (deg.)	Best $C_L^{3/2}/C_D$ from raw data
1.0	0.0708	4.22	3.43	5.7	3.56
3.0	0.0708	8.08	8.05	5.7	8.40
5.0	0.0708	10.97	11.78	5.7	12.20

Table 5. Six refined response surfaces for maximum $C_L^{3/2}/C_D$ as a function of y_c for Re = 2.0 ×10⁵ and Re = 8.0 ×10⁴ at AR = 1, 3, and 5.

	$Re=2\times10^5$	
$AR = 1$	$C_L^{3/2}/C_D = 4.159 - 0.0087y_c - 0.2064y_c^2 + 0.1345y_c^3$	$R^2 = 0.999, R_a^2 = 0.998, \hat{s} = 0.006$ (0.15% of mean)
$AR = 3$	$C_L^{3/2}/C_D = 9.790 - 0.1507y_c - 0.3234y_c^2 + 0.2713y_c^3$	$R^2 = 0.986, R_a^2 = 0.945, \hat{s} = 0.042$ (0.44% of mean)
$AR = 5$	$C_L^{3/2}/C_D = 14.21 - 0.0862y_c - 0.5541y_c^2 + 0.3984y_c^3$	$R^2 = 0.998, R_a^2 = 0.993, \hat{s} = 0.029$ (0.21% of mean)
	$Re=8\times10^4$	
$AR = 1$	$C_L^{3/2}/C_D = 3.550 - 0.1029y_c - 0.2177y_c^2 + 0.0807y_c^3$	$R^2 = 1.0, R_a^2 = 1.0, \hat{s} = 0.001$ (0.03% of mean)
$AR = 3$	$C_L^{3/2}/C_D = 8.454 + 0.0432y_c - 0.4117y_c^2 + 0.1803y_c^3$	$R^2 = 1.0, R_a^2 = 0.999, \hat{s} = 0.010$ (0.12% of mean)
$AR = 5$	$C_L^{3/2}/C_D = 12.22 + 0.2183y_c - 0.6310y_c^2 + 0.2483y_c^3$	$R^2 = 1.0, R_a^2 = 1.0, \hat{s} = 0.003$ (0.03% of mean)

Table 6. Optimal points selected by the six response surfaces in Table 5.

Re	*AR*	Optimal y_c	$C_L^{3/2}/C_D$ predicted	$C_L^{3/2}/C_D$ actual	Best $C_L^{3/2}/C_D$ from raw data
2.0×10^5	1	0.0396	4.16	4.15	4.15 @ y_c=0.04
2.0×10^5	3	0.0362	9.80	9.80	9.77 @ y_c=0.03
2.0×10^5	5	0.0386	14.22	14.20	14.19 @ y_c=0.04
8.0×10^4	1	0.0456	3.56	3.56	3.56 @ y_c=0.05
8.0×10^4	3	0.0411	8.46	8.45	8.45 @ y_c=0.04
8.0×10^4	5	0.0439	12.24	12.24	12.22 @ y_c=0.04

Table 7. Best reduced response surface for $C_L^{3/2}/C_D$ and predicted optimum for the first spanwise cross-section variation problem.

Response surface						
$C_L^{3/2}/C_D = 3.104 + 0.0839y_{cr} - 0.0199\alpha_r + 0.0340y_{ct} - 0.1048\alpha_t + 0.0779\alpha_r y_{cr} - 0.1245\alpha_r^2 - 0.0362y_{ct}y_{cr} + 0.0922\alpha_t y_{ct} - 0.1192\alpha_t^2$						
Statistical measures						
$R^2 = 0.777, R_a^2 = 0.642, \hat{s} = 0.127$ (4.34% of mean)						
Predicted optimum						
y_{cr}	α_r (deg)	y_{ct}	α_t (deg)	$C_L^{3/2}/C_D$ predicted	$C_L^{3/2}/C_D$ actual	Best $C_L^{3/2}/C_D$ from raw data
0.10	5.58	0.05	2.94	3.28	3.07	3.56

Table 8. Best reduced response surface for $C_L^{3/2}/C_D$ and predicted optimum for the second spanwise cross-section variation problem.

Response surface						
$C_L^{3/2}/C_D = 3.207 + 0.0250y_{cr} - 0.1029\alpha_r - 0.0559y_{ct} + 0.0173\alpha_t - 0.0765y_{cr}\,y_{cr} + 0.1906\alpha_r y_{cr} + 0.0212y_{ct}\alpha_r - 0.0275y_{ct}y_{ct} - 0.0147\alpha_t y_{cr} - 0.0408\alpha_t y_{ct} - 0.0332\alpha_t\alpha_t$						
Statistical measures						
$R^2 = 0.950, R_a^2 = 0.920, \hat{s} = 0.059$ (1.90% of mean)						
Predicted optimum						
y_{cr}	α_r (deg)	y_{ct}	α_t (deg)	$C_L^{3/2}/C_D$ predicted	$C_L^{3/2}/C_D$ actual	Best $C_L^{3/2}/C_D$ from raw data
0.05	5.0	0.05	5.0	3.49	3.56	3.56

Table 9. Best reduced response surface for $C_L^{3/2}/C_D$ and predicted optimum for the third spanwise cross-section variation problem.

Response surface						
$C_L^{3/2}/C_D = 3.328 + 0.1654y_{cr} - 0.0688\alpha_r + 0.0648y_{ct} - 0.0758\alpha_t - 0.1104y_{cr}\,y_{cr} + 0.1431\alpha_r y_{cr} - 0.0882\alpha_r\alpha_r - 0.0531y_{ct}y_{ct} + 0.0604\alpha_t y_{ct} - 0.1380\alpha_t\alpha_t$						
Statistical measures						
$R^2 = 0.933, R_a^2 = 0.897, \hat{s} = 0.087$ (2.88% of mean)						
Predicted optimum						
y_{cr}	α_r (deg)	y_{ct}	α_t (deg)	$C_L^{3/2}/C_D$ predicted	$C_L^{3/2}/C_D$ actual	Best $C_L^{3/2}/C_D$ from raw data
0.075	5.53	0.0565	4.8	3.42	3.35	3.56

Table 10. Five response surfaces for maximum $C_L^{3/2} \cdot S^{1/2}/C_D$ constructed from five successively refined sets (A-E) of design points for the fixed-span aircraft subject to the constraints of steady flight.

Set A	$C_L^{3/2}S^{1/2}/C_D = 1.154 + 0.1930y_c + 0.1115AR - 0.3642y_c^2 + 0.0097ARy_c - 0.0368AR^2$ $R^2 = 0.999, R_a^2 = 0.997, \hat{s} = 0.015$ (1.69% of mean)
Set B	$C_L^{3/2}S^{1/2}/C_D = 1.206 + 0.1960y_c + 0.0374AR - 0.3750y_c^2 + 0.0072ARy_c - 0.0073AR^2$ $R^2 = 0.999, R_a^2 = 0.999, \hat{s} = 0.006$ (0.63% of mean)
Set C	$C_L^{3/2}S^{1/2}/C_D = 1.139 - 0.0895y_c + 0.0433AR - 0.0236y_c^2 - 0.0004ARy_c - 0.0055AR^2$ $R^2 = 1.0, R_a^2 = 0.999, \hat{s} = 0.002$ (0.18% of mean)
Set D	$C_L^{3/2}S^{1/2}/C_D = 1.291 - 0.1739y_c - 0.4249y_c^2 + 0.3782y_c^3$ $R^2 = 0.981, R_a^2 = 0.923, \hat{s} = 0.069$ (6.40% of mean)
Set E	$C_L^{3/2}S^{1/2}/C_D = 1.263 + 0.0936y_c - 0.3127y_c^2 + 0.2002y_c^3$ $R^2 = 0.999, R_a^2 = 0.998, \hat{s} = 0.011$ (0.98% of mean)

Table 11. Predicted and actual maximum $C_L^{3/2} \cdot S^{1/2}/C_D$ with corresponding y_c obtained from the successively refined response surfaces presented in Table 10. AR = 1.5 for all designs.

Design Point Set	y_c	$C_L^{3/2} \cdot S^{1/2}/C_D$ predicted (meter)	$C_L^{3/2} \cdot S^{1/2}/C_D$ actual (meter)
A	0.0639	1.257	1.213
B	0.0635	1.263	1.215
C	0.0500	1.243	1.242
D	0.0416	1.307	1.256
E	0.0295	1.271	1.266

Table 12. Predicted and actual error comparisons for the predicted optimal points of Table 11.

Design Point Set	rms-error	standard error at optimum	actual error at optimum
A	0.015	0.011	0.044
B	0.006	0.004	0.048
C	0.002	0.002	0.001
D	0.069	0.051	0.051
E	0.011	0.007	0.005

Table 13. Best reduced response surface for maximum $C_L^{3/2} \cdot S^{1/2}/C_D$ fit to all of the design points in Sets A-E.

Response surface			
$C_L^{3/2}S^{1/2}/C_D = 1.153 + 0.1586y_c + 0.1504AR - 0.3786y_c^2 - 0.0465ARy_c$			
Statistical measures			
$R^2 = 0.919, R_a^2 = 0.897, \hat{s} = 0.080$ (7.87% of mean)			
Predicted optimum			
y_c	AR	$C_L^{3/2}S^{1/2}/C_D$ **predicted**	$C_L^{3/2}S^{1/2}/C_D$ **actual**
0.0574	1.5	1.311	1.226

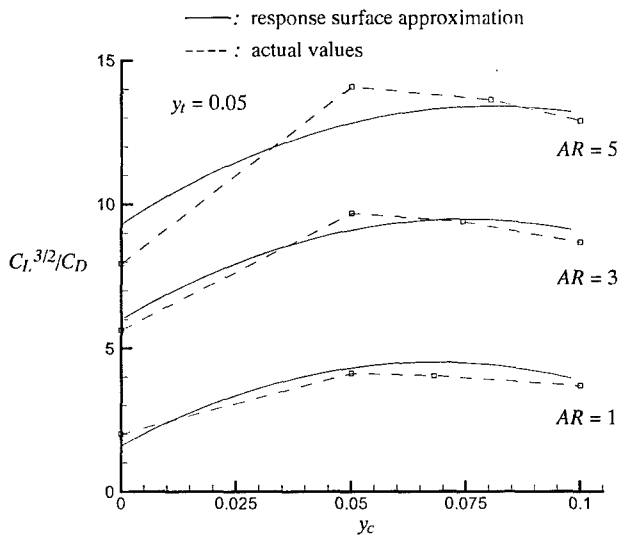

Figure 1. Actual and response surface approximation of $C_L^{3/2}/C_D$ vs. y_c for AR = 1, 3, & 5 at y_t = 0.05 and Re = 2.0 ×10^5.

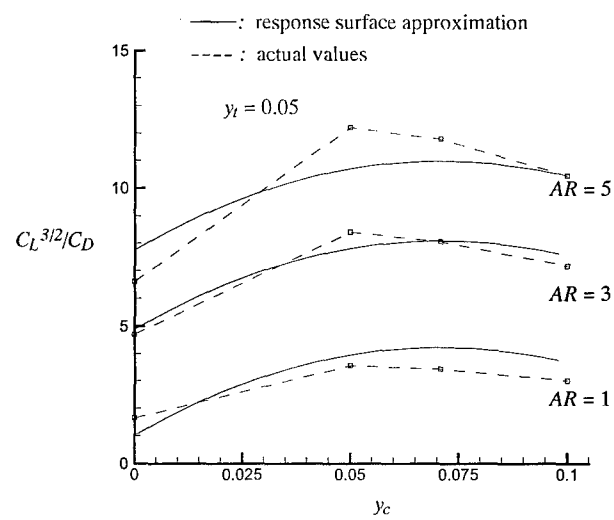

Figure 2. Actual and response surface approximation of $C_L^{3/2}/C_D$ vs. y_c for AR = 1, 3, & 5 at y_t = 0.05 and Re = 8.0 ×10^4.

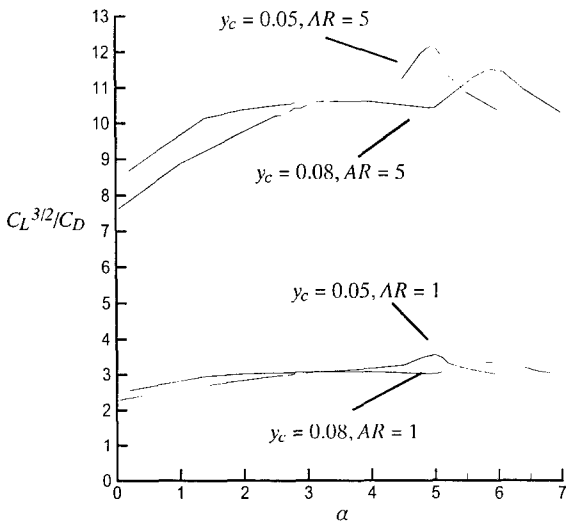

Figure 3. $C_L^{3/2}/C_D$ vs. α for four different wings representing aspect ratios of AR = 1 & 5 and cambers of y_c = 0.05 & 0.08.

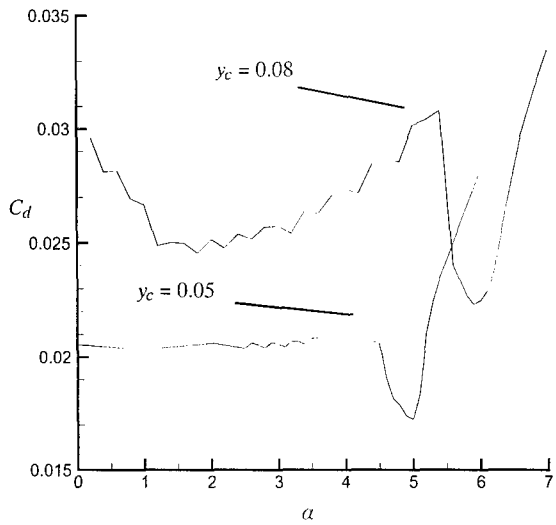

Figure 4. Profile drag coefficient, C_d, vs. α for both NACA 8405 and NACA 5405 airfoils.

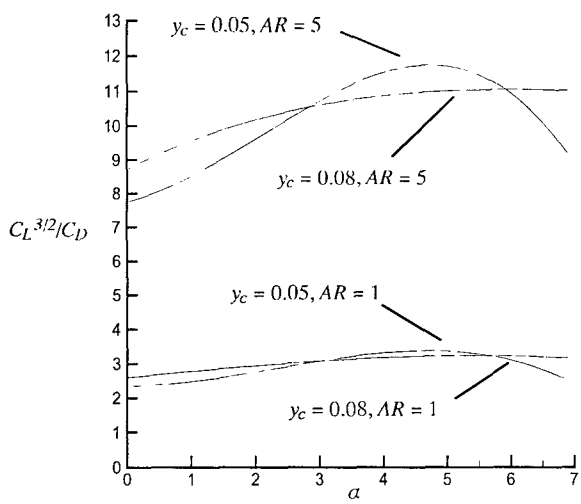

Figure 5. Quadratic polynomial approximations of the $C_L^{3/2}/C_D$ vs. α data in Figure 3 for the four different wings representing aspect ratios of AR = 1 & 5 and cambers of y_c = 0.05 & 0.08.

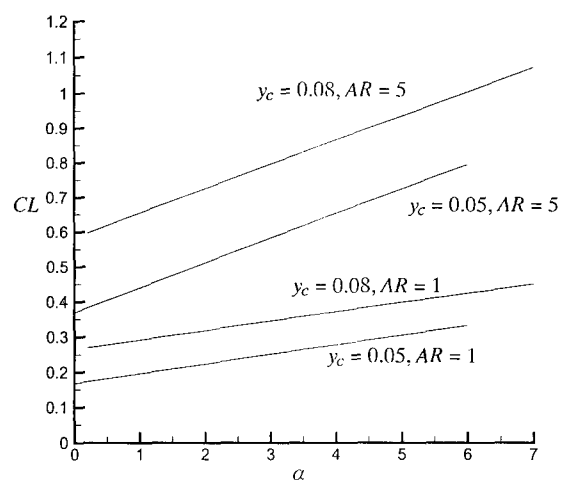

Figure 6. C_L vs. α for the four wings representing aspect ratios of AR = 1 & 5 and cambers of y_c = 0.05 & 0.08.

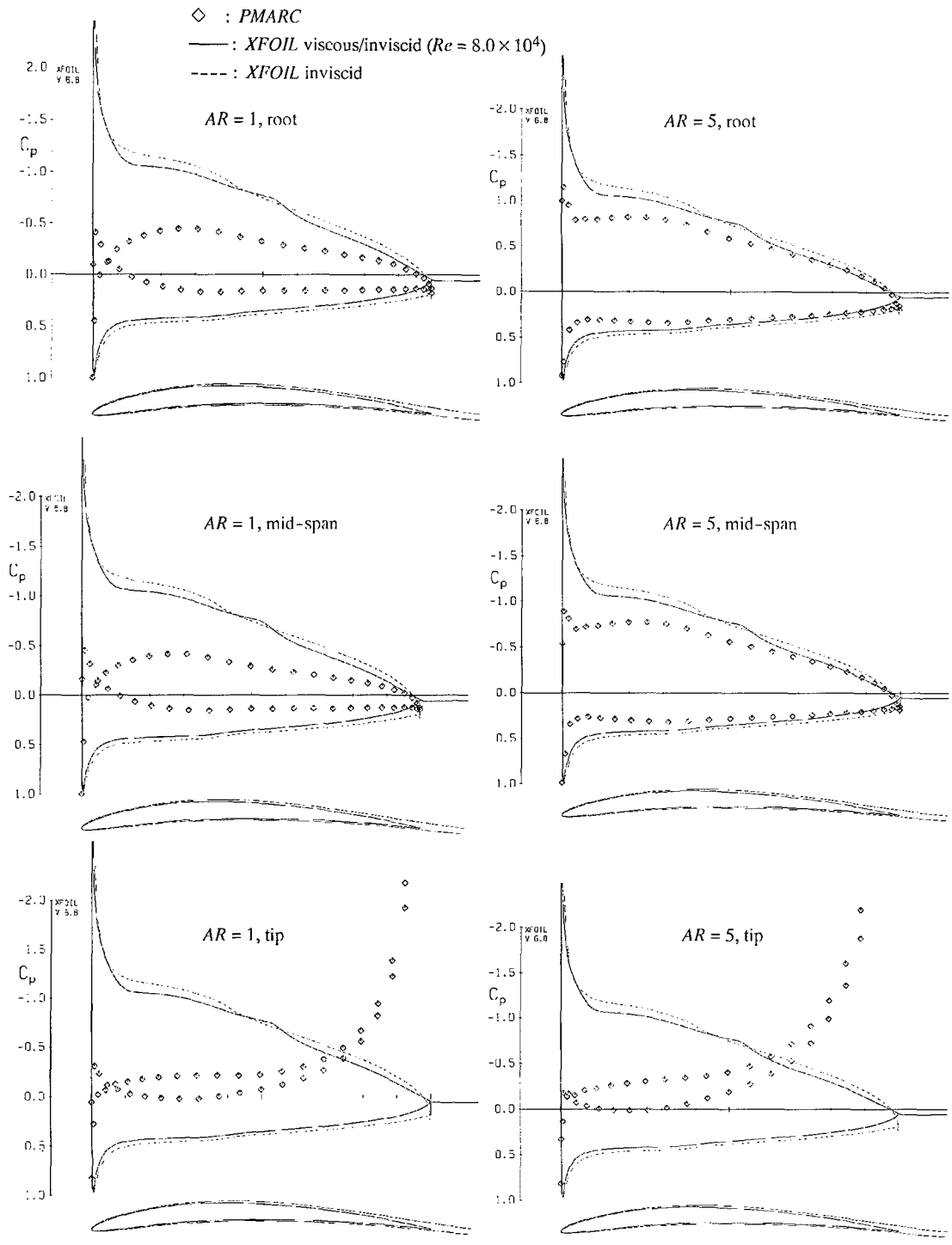

Figure 7. C_p distributions at the root, mid-span, and tip sections for a NACA 5405 airfoil at $\alpha = 5°$ for AR = 1 and AR = 5.

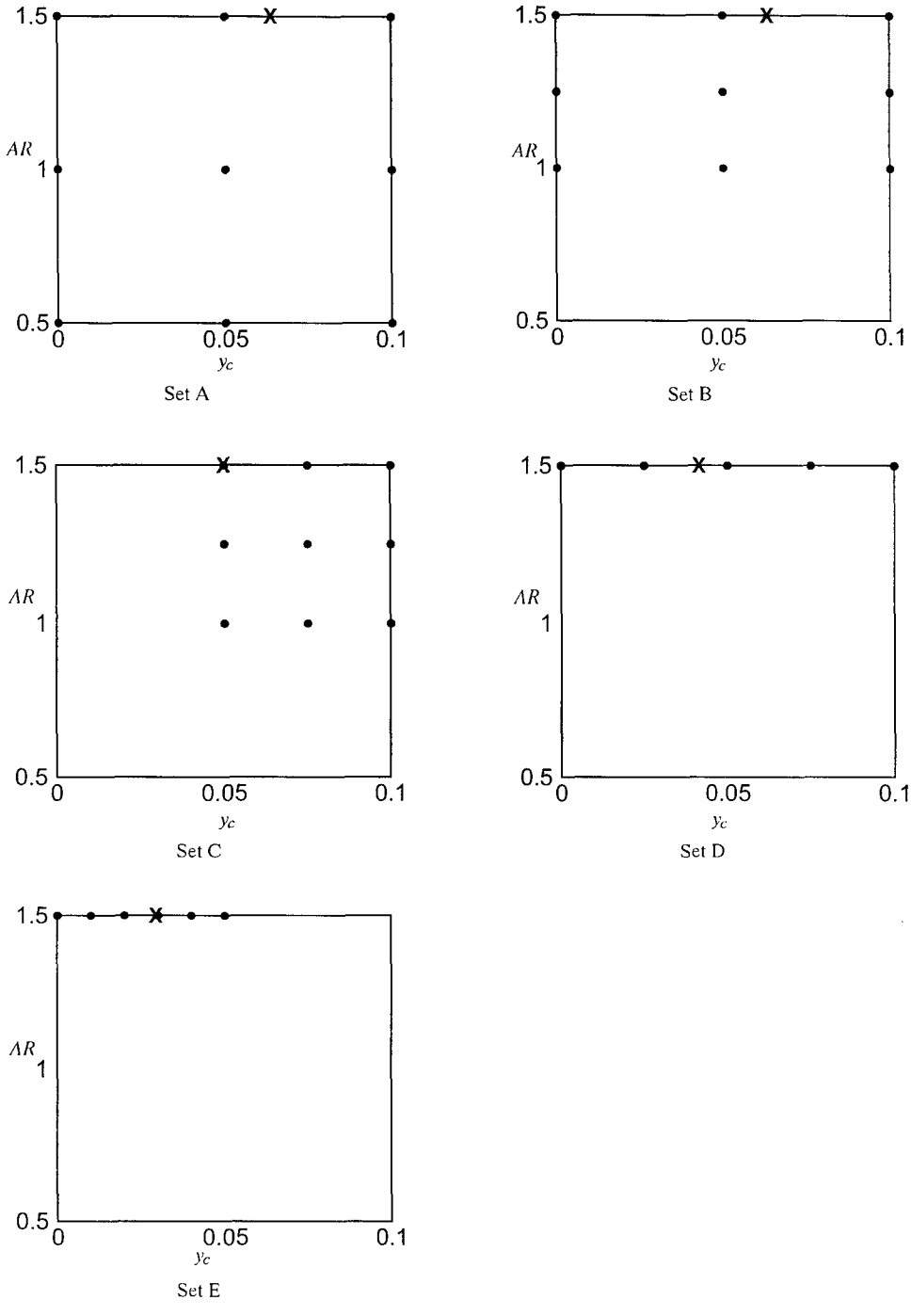

Figure 8. Five successively refined sets (A-E) of response surface design points. Circles mark the design points, and X marks the optimal point on the response surface selected by Solver.